Andes virus mRNA vaccines: comparison of unmodified and modified mRNA platforms

Alexander Bukreyev

abukreye@UTMB.EDU

University of Texas Medical Branch https://orcid.org/0000-0002-0342-4824

Ivan Kuzmin

University of Texas Medical Branch at Galveston

Ruben Soto Acosta

University of Texas Medical Branch at Galveston

Perry Wasdin

Vanderbilt Medical Center https://orcid.org/0000-0001-7351-2048

Chad Mire

University of Texas Medical Branch at Galveston

Taylor Engdahl

Vanderbilt Medical Center

Woohyun Moon

Aciotas

Vsevolod Popov

University of Texas Medical Branch at Galveston

James Crowe

Vanderbilt University Medical Center https://orcid.org/0000-0002-0049-1079

Ivelin Georgiev

Vanderbilt University Medical Center https://orcid.org/0000-0002-6312-7696

Mariano Garcia-Blanco

University of Texas Medical Branch at Galveston

Robert Abbott

University of Texas Medical Branch at Galveston

Article

Keywords:

Posted Date: August 10th, 2023

DOI: https://doi.org/10.21203/rs.3.rs-3182841/v1

Additional Declarations: Yes there is potential Competing Interest. Ivan Kuzmin, Mariano Garcia-Blanco and Alexander Bukreyev hold a patent for the Andes vaccines described in the manuscript.

Version of Record: A version of this preprint was published at Nature Communications on July 30th, 2024. See the published version at https://doi.org/10.1038/s41467-024-50774-3.

Abstract

Andes virus (ANDV) is a rodent-borne zoonotic orthohantavirus endemic in South America that causes hantavirus pulmonary syndrome in humans, with up to a 40% case fatality rate. We developed ANDV mRNA vaccines based on the M segment of the viral genome that codes for glycoproteins Gn and Gc in a single open reading frame of glycoprotein precursor (GPC). We generated RNAs either with regular uridine (U-mRNA) or N1-methylpseudouridine (m1Ψ-mRNA). Mice immunized by either ANDV U-mRNA or m1Ψ-mRNA developed similar germinal center responses in lymph nodes. Single cell RNA and BCR sequencing of germinal center B cells from vaccinated mice demonstrated similar levels of activation, except an additional cluster of cells exhibiting strong interferon response that was present in animals vaccinated with U-mRNA but not m1Ψ-mRNA. Furthermore, similar immunoglobulin class-switching and somatic hypermutations were observed for the two vaccines. Golden Syrian hamsters were immunized intramuscularly with 2 doses of the vaccines on days 0 and 21. The titers of Gn/Gc-binding antibodies were moderately greater for U-mRNA construct than for m1Ψ-mRNA construct, however, the titers of ANDV-neutralizing antibodies were equivalent. Vaccinated animals were challenged with a lethal dose of ANDV at 21 days after the boost, along with the naïve control group. All control animals succumbed to infection whereas all vaccinated animals survived without any detectable disease or viral load. The data demonstrate the development of effective vaccines against ANDV and the lack of a significant effect of m1Ψ mRNA modification on immunogenicity and protection in the hamster model.

INTRODUCTION

Hantaviruses (Family: *Hantaviridae*, Order: *Bunyavirales*) are negative-stranded, tripartite RNA viruses infecting fish, reptiles, and mammals [1]. Zoonotic hantaviruses of clinical significance belong to genus *Orthohantavirus*; they circulate in rodents and are transmitted to humans primarily by inhalation of aerosolized rodent excreta [2–4] followed sometimes by human-human transmission. Old World hantaviruses (such as Puumala, Hantaan, Seoul viruses) cause hemorrhagic fever with renal syndrome (HFRS) with case-fatality rates < 1–15%, depending on the specific causative agent, whereas New World hantaviruses cause hantavirus pulmonary syndrome (HPS) with case-fatality rates up to 40% [3]. Among the latter, the majority of human cases are caused in North America by Sin Nombre virus (SNV) and in South America by Andes virus (ANDV) [2,3].

Hantavirus genomes consist of three RNA segments: small (S), medium (M), and large (L). The S segment codes for nucleoprotein (N); the M segment codes for glycoproteins Gn and Gc in a single open reading frame of glycoprotein precursor (GPC); the L segment codes for polymerase protein (L) [5,6]. The synthetized GPC is cleaved to Gn and Gc by host signalases at pentapeptide motif WAASA [7]. Further, the cleaved Gn and Gc form heterodimer Gn/Gc complexes on the virion surface that interact with host cell receptors and trigger receptor-mediated endocytosis and further pH-driven membrane fusion via conformational changes of Gc [8,9]. It was shown that monoclonal antibodies directed to Gn or Gc of ANDV can efficiently neutralize the virus [10]. Orthohantavirus N is conserved, and viruses from various

species demonstrate antigenic cross-reactivity based on the N [11,12]. Glycoprotein cross-reactivity that causes cross-neutralization between certain hantaviruses was demonstrated as well, and serves as the basis of cross-protection elicited by hantavirus biologics [13–15].

No vaccines or preventive treatments for orthohantavirus infections have been approved by the US Food and Drug Administration (FDA) or the European Medicines Agency (EMA) to date. The only vaccines approved at the national level in China and in the Republic of Korea are inactivated whole-virion vaccines which elicit only moderate protection against Hantaan and Seoul viruses, respectively, but not against hantaviruses of other species [16,17]. In preclinical studies, vesicular stomatitis virus-vectored [18–20], human adenovirus type 5-vectored [21] vaccines against ANDV and SNV, and a vaccinia virus-vectored vaccine against Hantaan virus [15] have been reported. The most substantial efforts were focused on the development of DNA vaccines based on the M segment of the viral genome. DNA-vaccines targeting Old World hantaviruses, either mono- or polyvalent, have been evaluated in animals models [13,14,22–24] and underwent initial clinical trials [25–27]. These constructs were highly protective but suffered from the common limitation of DNA vaccines which is low immunogenicity and the resulting need to administer them several times at very high doses.

During recent years, substantial advance has been made in the development of mRNA vaccines against various pathogens [28–30], particularly during the COVID-19 pandemic [31–34]. The mRNA platform has multiple advantages: it is rapidly deployable, highly immunogenic, non-infectious, lacks a viral vector or another carrier which could induce undesirable immune responses, and lacks a risk of incorporation into the host's genome [35]. The mRNA vaccine constructs are often packaged in lipid nanoparticles (LNP), which serve multiple purposes: mRNA delivery into cell cytoplasm, protection from host nucleases, and adjuvant effects [35,36].

The immunogenicity of vaccines based on conventional mRNA may actually be reduced due to triggering toll-like receptors (TLRs) 3, 7, and 8, as well as RIG-I receptor resulting in strong induction of the innate immune response [37]. This leads to expression and activation of protein kinase R and 2'-5'-oligoadenylate synthase, which in turn leads to a strong suppression of translation of the intended vaccine [38]. In addition, induction of the innate immune response results in degradation of cellular and ribosomal RNA [38]. Several nucleoside modifications have been designed to combat induction of the innate immune response by mRNA. In particular, replacement of uridine with pseudouridine (e.g. N1-methyl-pseudouridine) has been shown to be the most effective [38,39]. It was suggested that cellular pattern recognition receptors (PRR) do not recognize the pseudouridine-containing RNA efficiently which results in reduced induction of the innate immune response, increased translation of the mRNA vaccine, and improved immunogenicity [28,29,39–41]. Additionally, triggering of the innate immune response occurs through recognition of double-stranded RNA which is synthetized as a by-product during *in vitro* production of mRNA by the bacteriophage T7 RNA-dependent RNA polymerase. This effect can be greatly reduced by incorporation of modified nucleosides [42].

On the other hand, non-modified mRNA vaccines also show promise. While the non-modified mRNA COVID-19 HERALD vaccine platform was discontinued by CureVac, it met the prespecified success criteria for efficacy against COVID-19 despite the low 12 µg mRNA dose [43], which is lesser than that of BNT162b2 (30 µg) and Moderna (100 µg) COVID-19 vaccines. Therefore, the unmodified mRNA vaccine platform is also actively pursued [44,45]. Successful use of some PRR agonists as adjuvants for protein-based vaccines (reviewed in ref. [46]) further supports the argument that induction of innate immune responses by non-modified RNA may be beneficial for the overall vaccine immune response. It is possible that while the innate immune response to nonmodified mRNA inhibits the translation, it also stimulates immune cells such as dendritic cells, T cells and B cells for better adaptive immune response [47,48]. Thus, the net effect of vaccine RNA modification can only be evaluated by a direct comparison of a non-modified and modified mRNA vaccines which otherwise are identical.

In the present study, we focused on the development and evaluation of mRNA vaccines against ANDV because of its public health significance and lack of licensed vaccines. ANDV caused a human outbreak with aggressive airborne human-to-human transmission and multiple fatalities in 2019–2020 [49], highlighting its epidemic and pandemic potential. We generated mRNA vaccines based on non-modified and modified mRNA platforms which were otherwise identical. The two ANDV vaccines were compared for protein expression, innate immunogenicity *in vitro*, induction of germinal centers, antibody responses, activation of B cells, BCR repertoires and the protective efficacy *in vivo* in a 100% lethal animal model.

RESULTS

Design of the ANDV GPC mRNA vaccine construct

Analysis of 70 complete ANDV M segment sequences available in GenBank demonstrated high conservation of the glycoprotein precursor (GPC) amino acid sequences, with identity values ranging 98.4–100%. The most divergent sequences had only 5 amino acid substitutions that occurred randomly in the domains corresponding to Gn and Gc. We selected the well characterized reference sequence NC_003467 for our construct. The 5’ non-coding region of the mRNA originated from the same viral genome which possessed the required minimum Kozak sequence [50]. The open reading frame (3,417 nucleotides including stop-codon) was optimized for expression in human cells using GenSmart Codon Optimization algorithm available at GenScript, with G + C content of 56.13%, and avoidance of restriction sites used for insertion of the construct into plasmid and its linearization. This open reading frame was followed with a 3’ non-coding region that consisted of two head-to-tail concatenated sequences of human genomic origin, partial mitochondrially encoded 12S rRNA (mtRNR1) and amino-terminal enhancer of split (AES), a combination that was demonstrated to enhance protein expression from various mRNAs [51]. The 3’ UTR sequence was followed by a poly-A tail of 120 nucleosides, and restriction sites EcoRV and BstBI separated by a 30-nucleoside poly-A stretch, that were used for linearization of the DNA template. The construct (Fig. 1A) was cloned under T7 promoter with an addition of the GGC sequence upstream of the 5’ viral sequence to improve the transcription efficiency.

After linearization of the DNA template with EcoRV and BstBI restriction enzymes, *in-vitro* transcription was conducted using either the regular uridine (U-mRNA) or N^1-methylpseudouridine (m1Ψ-mRNA) to generate products with different nucleoside compositions, and cap-1 was added co-transcriptionally. The RNAs were dephosphorylated and purified with cellulose [52].

While the m1Ψ modification of mRNA prevents the effective innate immune response, its effect on the translation is marginal

We evaluated the expression of Gn/Gc in A549 cells at 24 h post transfection with either U-mRNA or m1Ψ-mRNA in equal concentrations by flow cytometry using a cocktail of human monoclonal antibodies that are capable to bind ANDV Gn/Gc antigen and neutralize ANDV *in vivo*[10], with FITC-labeled secondary antibody. The results demonstrated effective expression of the antigen in cells transfected with either construct (Fig. 1B, C). Proportion of cells expressing Gn/Gc from m1Ψ-mRNA (mean 55.1%; CI_{95} 52.4–57.7%) was greater than from U-mRNA (mean 43.3%; CI_{95} 37.9–48.7%), and the median fluorescence intensity (MFI) of FITC signal from cells transfected with m1Ψ-mRNA (mean 87169.5 reactive units [RU]; CI_{95} 77589.9–96748.7RU) was statistically greater than the MFI of cells transfected with U-mRNA (mean 54969.33RU; CI_{95} 47025.1-62913.6). Nevertheless, the overall difference between the levels of expression from the two vaccine constructs was modest.

To compare the innate immune response triggered by the constructs, A549 cells were transfected with either U-mRNA or m1Ψ-mRNA, harvested in 24 h, and mRNA transcripts were evaluated by quantitative RT-PCR using TaqMan™ Array, Human Cytokine Network, pre-defined and custom (Applied Biosystems). In total, expression of 48 genes were evaluated by ΔΔCt algorithm with 18S or GAPDH as housekeeping genes. Among type I interferons, only IFNβ was detected and could be measured comparatively; type II interferon (IFN) was not expressed in A549 cells under any treatment; and type III interferons (IFNλ1, IFNλ2, IFNλ4) were expressed in the cells transfected with U-mRNA but not in the mock-transfected cells or in the cells transfected with m1Ψ-mRNA. In addition to interferons, 14 interferon-stimulated and other innate immune genes were overexpressed in the cells transfected with U-mRNA but none of these transcripts were detectable in the cells transfected with m1Ψ-mRNA. These data demonstrate that U-mRNA triggers effective innate immune response, while m1Ψ-mRNA does not (Fig. 1D), which is consistent with previous reports [37].

The expressed ANDV Gn/Gc self-assemble into virus-like particles (VLP) or large protein aggregates

Previous studies reported that glycoproteins of bunyaviruses [53] including hantaviruses [54] can self-assemble into virus-like particles (VLPs) in the absence of other viral proteins. We were interested to assess whether ANDV Gn/Gc expressed from our mRNA constructs are capable to form VLPs. Clarified supernatant from 293T cells transfected with ANDV mRNA was concentrated 250x by ultracentrifugation at 100,000 x g and evaluated via transmission electron microscopy with uranyl acetate counterstaining. The observed roughly-rounded structures were compatible to hantavirus particles, 56–95 nm in diameter

(mean 72 nm, CI_{95} 65.6–78.4), and their specificity was further confirmed by immunogold staining (Fig. 1E). However, we did not observe the surface grid-like pattern [55,56] as well as structures resembling membrane envelope and surface projectiles typical for ectodomain spikes on hantavirus virions [56–59]. Therefore, we cannot completely rule out the possibility that Gn/Gc complexes formed large protein aggregates rather than VLP. Negative control specimens evaluated by the same method did not show positive immunostaining. It is possible that a formation of VLP or large glycoprotein aggregates with particulate presentation of the antigens improve immune response, although we only demonstrated these structures *in vitro* and do not know if the same occur in vaccinated animals.

m1Ψ modification of mRNA does not affect significantly the germinal center response in draining lymph nodes

The majority of vaccines work by inducing protective antibody responses [60]. To produce these antibody responses, antigen-activated B cells rapidly proliferate and enter germinal centers (GC) during the days following vaccination [61]. The GC are specialized microstructures in lymph nodes where B cell clones undergo further differentiation [62], somatically mutate their B cell receptors (BCR), and develop affinity-matured protective antibodies in the weeks following vaccination [62]. Therefore, it is critical to evaluate how efficient novel vaccine constructs can induce GC responses.

To assess the ability of our mRNA vaccine constructs to induce GC responses, 10–12 week old C57Bl6/J mice were immunized intramuscularly with a single dose (5 µg) of either U-mRNA, Ψ-mRNA vaccine (LNP-encapsulated), or a recombinant Gn^H/Gc antigen [8] mixed with alum (Alhydrogel 2%). Naïve mice were also assessed as a negative control. On day 12 following vaccination we observed a statistically significant induction of germinal centers in all vaccine groups by flow cytometric analysis (Fig. 2A). Germinal centers were gated as $GL7^+CD38^-$ among all live B cells in the draining lymph nodes (Fig. 2B). The magnitude of this response was comparable between the vaccine groups as measured by the frequency of total B cells or assessed by absolute number (Fig. 2C,D). Taken together, these results suggest both ANDV mRNA vaccine constructs were equally capable of inducing GC B cell responses *in vivo*.

m1Ψ modification of mRNA does not significantly affect the transcriptional activation of germinal center B cells in draining lymph nodes

Type I interferons produced by dendritic cells promote their phenotypic and functional activation [63] and also promote expansion and differentiation of T lymphocytes and antibody-producing B cells [64]. As the U-mRNA vaccine but not the m1Ψ-mRNA vaccine induced type I interferon response (Fig. 1B), we were interested to compare the activation of germinal center B cells in draining lymph nodes after the vaccination. We used BALB/c mice for single-cell sequencing because they mount a more robust antibody response as compared to C57BL/6 mice [65], and the number of isolated germinal center B cells could be a limiting factor for single-cell sequencing. Groups of 10-week-old BALB/c mice were

immunized intramuscularly (IM) with a single dose (25 μg) of ANDV mRNA vaccines or 20 μg of ANDV Gn^H/Gc-Alum antigen as a protein vaccine control. A separate group of mice were vaccinated with empty LNP to serve as negative controls. Twelve days post vaccination the animals were euthanized, their popliteal and inguinal lymph nodes harvested, germinal center B cells were purified by FACS and subjected to single-cell RNAseq (Fig. 3A) except the negative control (empty LNP) where germinal centers were not observed and unpurified lymphocytes were used instead. As expected, uniform manifold approximation and projection (UMAP) and principal component analysis (PCA) (Fig. 3B, S1A,B) showed that unpurified lymphocytes from mice that were mock immunized with empty LNP formed a separate group in the UMAP and fell along a distinct axis in the PCA. Germinal center B cells from mice immunized with either U-mRNA, m1Ψ-mRNA, or Gn^H/Gc overlapped in the UMAP projection, suggesting similar transcriptional profiles. Unsupervised clustering of these cells further supported these observations, as cells from mice sham-immunized with empty LNP formed a unique cluster. The rest of the clusters all contained a mixture of cells across the treatment groups, except for cluster 9, which almost exclusively (92%) contained cells from mice immunized with U-mRNA vaccine. Although in general there were no significant differentially expressed genes between the groups of immunized mice (Fig. S1C), the cluster 9 demonstrated upregulation of genes and enrichment of pathways involved in the innate immune response (Fig. S1D). The upregulation of genes in cluster 9, which was induced only by the U-mRNA vaccine is consistent with the proinflammatory transcriptional profile of this vaccine in transfected A549 cells (Fig. 1B). However, the overall transcriptional profile of the germinal center B cells based on all 11 clusters looked similar for the two vaccines.

Next, expression of common B cell activation markers was compared across treatment groups (Fig. 3C). As expected, unpurified lymphocytes from the empty LNP control group showed little or no activation of these markers expressed by B cells. Some activation of the markers (particularly CD79B) was consistent with immunostimulatory effects of LNP [36]. Both groups vaccinated with the two mRNA vaccines demonstrated a strong upregulation of multiple markers of activation, particularly CD79B, as well as CD83 and AICDA, and overall showed almost identical expression of the markers. The B cells from mice vaccinated with the Gn^H/Gc protein showed lower mean expression of CD79B and slightly higher mean expression of CD83 compared to the mRNA vaccine groups. Overall, these data demonstrate that despite the strong suppressive effect of the m1Ψ modification on the innate immune response (Fig. 1B), the modification had only marginal effects on the activation of lymph node germinal center B cells.

The vaccine mRNA may be detectable in vaccinated mice during several days post immunization [66,67], and in the germinal centers of human lymph nodes up to two months [68]. We therefore were interested to check if the vaccine mRNA was detectable in the germinal centers of mouse lymph nodes. The vaccine mRNA was detected in all mice across the two vaccinated groups (Fig. 3D). The percentages of cells retaining any amount of the transcripts varied highly across mice within and between vaccine groups, ranging from 0.4–5.2% of the total B cells in each mouse although in general this proportion tended to be greater in mice vaccinated with m1Ψ-mRNA. The germinal center B cells containing the vaccine RNA were uniformly distributed across the UMAP projection of the scRNA-seq data and appeared in small

proportions of cells within every cluster including across B cells with all heavy chain isotypes. For example, we did not find a greater proportion of cells containing the vaccine RNA in cluster 9 which exhibited overexpression of innate immune genes. Persistence of vaccine antigen may be a beneficial overall aspect of mRNA vaccines, as extended release regimens have been shown to potentiate germinal center responses [69,70]. However, further detailed studies are needed to determine if the recovered mRNA is actually within germinal center B cells (vs mRNA LNPs that may be surface bound to B cells) and the significance of the persistence of vaccine RNA following vaccination.

ANDV U-mRNA and m1Ψ-mRNA vaccines induce equal class-switching and somatic hypermutation in draining lymph nodes

As discussed above, type I interferons promote phenotypic and functional activation of dendritic cells and promote expansion and differentiation of the adaptive immune response. We therefore sought to compare the difference in class-switching and somatic hypermutation in germinal center B cells from draining lymph nodes following vaccination with U-mRNA (high innate immunogenicity) and m1Ψ-mRNA (low innate immunogenicity) in mice. To achieve this, we performed single-cell BCR sequencing of RNA isolated from FACS-purified germinal center B cells recovered from draining lymph nodes on day 12 after vaccination in the mouse study shown in Fig. 3A. As expected, compared to the unpurified lymphocytes from the control mock-vaccinated LNP only group, the two mRNA vaccines increased the proportion of germinal center B cells positive for IGHG1, IGH2B, IGH2C and IGH3, but reduced the proportion of cells positive for IGHM, suggesting induction of a balanced Th1/Th2 response. Similar to the B cell transcriptional activation profiles (Fig. 2C), no difference was detected between the two mRNA vaccines. In contrast, vaccination with Gn^H/Gc-Alum demonstrated increased proportion of IGHG1 and only negligible proportion of IGHG2B, HGHG2C and IGH3 consistent with induction of Th2 response by this adjuvant.

The CDRH3 length did not change across any of the treatment groups (Fig. 4A,B), and no difference in clonal diversity was observed. The comparisons of mean proportion of somatic hypermutation (SHM) yielded no difference between the U-mRNA and m1Ψ-mRNA groups although SHM in both groups of mice were higher than in the unpurified empty LNP group as expected. SHMs in both mRNA vaccinated groups trended to be higher than in the Gn^H/Gc-Alum vaccinated group, although did not reach statistical significance (Fig. 4C, S3). Overall, these data demonstrate that even though the m1Ψ modification effectively reduces induction of the innate immune response, the modification does not affect the class-switching and induction of SHMs in draining lymph node germinal center B cells.

Both LNP-encapsulated U-mRNA and m1Ψ-mRNA vaccines elicit potent Gn/Gc-binding and virus-neutralizing antibody responses in golden Syrian hamsters

Groups of golden Syrian hamsters were immunized or mock-immunized intramuscularly with 25 μg of ANDV mRNA constructs encapsulated in LNP on days 0 and 21 (Fig. 5A), and challenged with ANDV on

day 42 (21 days after the boost). The animals were observed until day 28 post challenge (dpc). Blood serum was collected at days 0 (baseline), 21 (pre-boost), 41 (pre-challenge), and 70 (terminal, 28 dpc).

Serum IgG binding to ANDV glycoproteins (Gn/Gc-IgG) were determined in ELISA with recombinant Gn^{H}/Gc antigen [8] starting from serum dilution 1:100. Twenty-one days after the first vaccination, 4 out of 5 hamsters immunized with U-mRNA vaccine demonstrated Gn/Gc-IgG in serum dilutions 1:100 to 1:400 whereas one hamster had IgG titer of 1:4,800 (Fig. 5B). Hamsters immunized with m1Ψ-mRNA vaccine did not have detectable Gn/Gc-IgG at that time. After the boost, Gn/Gc-IgG titers increased not only in animals immunized with the U-mRNA vaccine, but animals immunized with the m1Ψ-mRNA vaccine responded as well, although to lesser titers (Fig. 5B).

ANDV-neutralizing antibodies in hamster sera were determined in plaque reduction assay (Fig. 5C). On day 21 after the first vaccination, 2 out of 5 animals in each group showed low but detectable neutralizing antibody titers. We detected 50% plaque reduction neutralization titers (PRNT50) of 28.3 and 64.1 for hamsters immunized with U-mRNA vaccine, and 33.1 and 36.2 for hamsters immunized with m1Ψ-mRNA vaccine. After the boost, all vaccinated hamsters in both groups developed detectable neutralizing antibody titers. In animals immunized with U-mRNA vaccine, the PRNT50 values were 48.9-263.3 (mean 141.6; CI_{95} 66.0-217.2), and in animals immunized with m1Ψ-mRNA vaccine the PRNT50 values were 83.5-245.4 (mean 164.5; CI_{95} 83.5-245.4). While the titers of ANDV-neutralizing antibody responses were greater for the non-modified mRNA-based vaccine, the difference was relatively small. These data suggest that both vaccines induced potent antibody responses and did not show any benefit of the mRNA modification.

Given previous reports on cross-neutralization between ANDV and SNV [13,14,18], we evaluated hamster sera collected 21 days after the boost for neutralization of SNV (Fig. 5D). Four out of five animals immunized with U-mRNA vaccine, and two out of five animals vaccinated with m1Ψ-mRNA vaccine demonstrated SNV-neutralizing activity (PRNT50 31.3–56.6).

Both LNP-encapsulated U-mRNA and m1Ψ-mRNA vaccines equally protect hamsters from the disease and death cause by ANDV

Hamsters were challenged intramuscularly with 250 PFU of ANDV on day 21 after the booster vaccination (Fig. 6A). This dose was demonstrated to be uniformly lethal in our previous studies [10,71]. The control animals started showing abrupt disease signs on 9 dpc (lack of movement and reactions to experimenter, hunched posture, rapid shallow breathes) and were euthanized within 24 h with progressive severe respiratory distress. Upon necropsy, large amounts of liquid were found in hamster thorax indicative for pulmonary edema. In contrast, all vaccinated animals survived until the end of observation (28 dpc) without signs of disease including changes of body weight or temperature (Fig. 6B,C, S4). Liver and lung tissues were collected at necropsy, and high titers of ANDV were detected in livers of all control animals and lungs from 3 out of 5 control animals. In contrast, no virus was isolated from the liver or lungs of any vaccinated animal (Fig. 6D,E).

The infectious challenge further boosted the neutralizing antibody titers. Surprisingly, the control mock-vaccinated hamsters (based on three samples available for testing) also developed high neutralizing antibody titers after the challenge, although the duration of incubation periods was 9 days only, and the duration of the disease was no longer than 24 h before the animals were euthanized. These samples were negative in the Gn/Gc-IgG ELISA (Fig. 5B) suggesting that immunoglobulins of other classes (for example, IgM) or alternative epitopes not detected by ELISA might mediate virus neutralization. Nevertheless, this failed to protect the non-vaccinated animals from lethal disease.

To further determine if sterilizing immunity was likely achieved, we tested sera of hamsters collected on day 28 after the challenge for antibodies binding to viral nucleoprotein (N) in ELISA. High titers of N-binding antibodies were suggested to be indicative for virus replication upon challenge [23,24]. We used recombinant truncated N protein of Puumala virus that was shown to cross-react with ANDV N protein [24,72]. The post-challenge data demonstrated no or low N-specific antibodies compared to the positive control that originated from hamsters surviving ANDV infection in our previous experiments (Fig. 6F) suggesting no significant replication of ANDV in vaccinated animals. Overall, these data demonstrate excellent protective efficacy of the two vaccines and lack of any detectable effect of RNA modification on the protection.

DISCUSSION

Hantaviruses pose a significant public health threat in parts of the world, and their pandemic potential was highlighted by human-to-human airborne transmission of ANDV in 2019–2020 [49]. They are prevalent in Asia, and millions of doses of inactivated vaccines against Hantaan and Seoul viruses have been deployed in China and in the Republic of Korea with limited success [16]. In the New World, the prevalence of zoonotic hantaviruses is less, but the severity of human disease is greater, with up to 40% case fatality rates [3]. It is important to note that the emergence of ANDV and SNV was documented relatively recently, in the 1990s [2], likely due to a combination of anthropogenic factors bringing humans to close contact with rodents, and favorable factors for proliferation of rodent populations in proximity to humans [3,16]. Humankind has learned hard lessons about emerging zoonotic pathogens, including those from the COVID-19 pandemic. There is no guarantee that New World hantaviruses may not cause a similar pandemic in the future, even though at present a large-scale deployment of ANDV or SNV vaccines does not look justified. Furthermore, once we have a successful technology for one of these pathogens, we likely can adapt it to others, including Old World hantaviruses, as was done with DNA vaccines in the past [11,13,22].

The success of the m1Ψ-mRNA modification led to its incorporation into several mRNA vaccines [31,32,34,73,74]. Additionally, mRNA constructs based on non-modified nucleosides in other studies were capable to elicit robust immune response and protection in various animal models [45,75–77]. However, as mRNA vaccine technology is still rather new, a direct side-by-side experiential comparison of the two vaccine platforms is required for their comprehensive evaluation. Here we generated two otherwise

identical mRNA constructs incorporating uridine (U-mRNA) or N^1-methylpseudouridine (m1Ψ-mRNA). We used 5' non-coding sequence of viral origin as was done previously in hantavirus DNA vaccines [13,23,24,78], although some mRNA studies suggested that a better protein expression may be achieved if eukaryotic (e.g. human) 5' UTR is used upstream in the protein coding sequence [44,79,80]. Further studies are needed to evaluate whether the use of human genomic 5' UTR would improve hantavirus protein expression in human cells. We used a human-derived 3' UTR previously reported to improve protein expression [51]. Obviously, all these elements are potential subjects of further optimization, along with the length of the poly-A tail, addition of nucleotide spacers, specific residues for folding optimization, and other sequence modifications [28,30,81]. The ANDV Gn and Gc glycoproteins expressed from a single open reading frame were successfully cleaved in cells and assembled into the typical Gn/Gc structures that were detected by ANDV antibodies. In animal studies, we employed mRNA encapsulated in LNP which not only protect mRNA from fast degradation but also serve as a potent adjuvant [36].

The m1Ψ-mRNA construct demonstrated lack of a significant innate immune response *in vitro*, in contrast to U-mRNA, which induced a strong innate response (Fig. 1B, Table S1). This observation is in line with previous publications which demonstrated that mRNA composed of modified nucleosides, and particularly of N^1-methylpseudouridine, is not recognized by cellular toll-like receptors which results in a reduced type I IFN response, increased translation, and improved adaptive immune response [37,40]. However, despite the high innate immunogenicity of U-mRNA, the level of expression of GPC from this construct was only moderately reduced in transfected cells, as compared to m1Ψ-mRNA (Fig. 1C,D). Furthermore, both constructs induced equal formation of germinal centers (Fig. 2), comparable class-switching and somatic hypermutation in B cells in draining lymph nodes (Fig. 4), and equal immunogenicity (Fig. 5). Comparison of B cell activation also demonstrated very similar profiles for the two vaccines, except the presence of the cluster 9 with upregulation of genes and enrichment of pathways involved in the innate immune response in mice immunized with the U-mRNA vaccine only (Fig. 3, S1).

Golden Syrian hamsters are very susceptible to ANDV that causes fast progressing disease and kills animals within hours after the clinical onset. The viral dose that we used was uniformly lethal to naïve animals in the present and previously published studies [71,82]. In contrast, animals immunized with either vaccine were protected from death and did not show any signs of clinical disease or detectable viral load in the liver or lungs. We documented no or barely detectable IgG specific to viral N protein in their sera, likely suggesting a lack of replication of the challenge virus.

Serum samples from several ANDV-immunized hamsters cross-neutralized SNV, and the same was reported previously for vectored vaccines [18]. We do not know whether the immune response elicited by our ANDV vaccine would be protective against SNV upon challenge as it cannot be evaluated easily in a conventional rodent model.

Why did the m1Ψ-U modification have only a relatively modest effect on the protein expression (Fig. 1C,D) and no effect on immunogenicity (Fig. 2, 3, 4, 5) and protective efficacy (Fig. 6) despite the strong suppressive effect on the innate immunogenicity? Several explanations can be suggested. First, the extent of interferon-mediated activation of protein kinase R and 2'-5'-oligoadenylate synthetase (which inhibit the translation) varies broadly, and possibly is not very significant in A549 cells used to compare the expression in this study (Fig. 1C,D) and in immune cells involved in presentation of the antigen *in vivo*, such as B cells (Fig. 4) and dendritic cells. Second, the relevant cell types may have additional mechanisms which minimize the inhibitory effects of the innate response on the translation. Third, it is also possible that a reduced expression of antigen from non-modified mRNA is compensated by the immunostimulatory effects of the cytokines induced by non-modified but not by modified form of mRNA. It should be noted that we cannot completely exclude a possibility that we could see benefits of the m1Ψ-U modification if the vaccine is tested at a much lower dose, although the greater induction of ANDV-specific IgG by U-mRNA as compared to m1Ψ-mRNA (Fig. 5B) argues against this possibility. Furthermore, IL-1 and IL-1ra are key regulators of the inflammatory response to RNA vaccines which are different in human and rodent cells [83]. Nevertheless, demonstration of high immunogenicity and protective efficacy of non-modified mRNA vaccines in non-human primates [44,45], and tolerability in human trials [43], indicates the high potential of this vaccine platform.

METHODS

Viruses used in the study. ANDV, isolate Chile-9717869 (GenBank accession No AF291703, NC_003467), recovered in 1997 from a long-tailed pygmy rice rat (*Oligoryzomys longicaudatus*), was used after 8 passages in Vero E6 cells. SNV, isolate SN 77734 (GenBank Accession No AF281850), recovered in 2006 from a deer mouse (*Peromyscus maniculatus*), New Mexico, USA, was used after 2 passages in deer mouse and 4 passages in Vero E6 cells.

Production of DNA template for ANDV mRNA. Nucleotide sequence of 5' untranslated region and open reading frame (ORF) was obtained from the reference ANDV M segment sequence, GenBank record NC_003467. The ORF was codon-optimized using GenSmart Codon Optimization, Version Beta 1.0 available at GenScript website (https://www.genscript.com/tools/gensmart-codon-optimization; last time accessed on February 15, 2022). Partial mtRNR1 (mitochondrially encoded 12S rRNA) and AES (amino-terminal enhancer of split) sequences concatenated head-to-tail, used for 3' untranslated region, were described elsewhere [51]. Poly-A tail of 120 nucleotides was placed downstream, and restriction sites NotI, EcoRV, and BstBI were incorporated for insertion of the construct into plasmid and further linearization. The sequence was placed under T7 promotor with the addition of GGC codon to improve transcription efficiency. The construct was generated by GenScript and supplied in pUC-19 vector.

Plasmid amplification was performed in NEB Stable competent cells (New England Biolabs), selected clones were sequenced prior to use. The template purified with ZymoPURE Plasmid Maxiprep kit (Zymo Research) was linearized using EcoRV and BstBI restriction enzymes (New England Biolabs).

mRNA generation, purification, and encapsulation. Two mRNA constructs were prepared from the same DNA template, one with regular uridine (U-mRNA) and another with N^1-methylpseudouridine (m1Ψ-mRNA). We followed the protocol published previously [84]. The U-mRNA was generated using HiScribe In-vitro Transcription Kit (New England Biolabs) with CleanCap Reagent AG (TriLink) to obtain cap-1 structure. The m1Ψ-mRNA for in-vitro studies was generated per the same protocol with the only difference that uridine was replaced with N^1-methylpseudouridine (TriLink). The m1Ψ-mRNA for *in vivo* study in Syrian hamsters was generated using HighYield T7 Cap 1 AG (3'-OMe) mRNA Synthesis Kit (me1Ψ-UTP) (Jena Bioscience GmbH). The generated RNA was purified with lithium chloride [85] and dephosphorylated with recombinant shrimp alkaline phosphatase (New England Biolabs). Further mRNA was purified from dsRNA contaminants by cellulose as described previously [52], and finally precipitated with sodium acetate [85]. DNA template and RNA concentrations were determined using NanoDrop instrument (ThermoFisher Scientific). The purified RNA was either used in *in vitro* studies or encapsulated into LNP of proprietary formulation by Acuitas Therapeutics (Vancouver, BC, Canada) for subsequent *in vivo* experiments.

On different steps of preparation, RNA integrity was assessed by electrophoresis on 2% agarose (E-Gel EX, Invitrogen), whereas the presence of dsRNA contaminants prior and after cellulose purification was assessed with J2 monoclonal antibody (Millipore Sigma) via dot-blot on BrightStar Plus positively charged nylon membrane (Invitrogen), further incubated with a secondary goat anti-mouse HRP-conjugated antibody (SeraCare), developed using Pierce ECL 2 Western Blotting Substrate (Thermo Scientific), and detected on Odyssey ® XF Imaging System (LI-COR).

Transfection of cells with ANDV mRNA. A549 or 293T cells grown in 24-well plates during 24 h for 70–90% confluence were transfected with 0.5-1.0 µg of cellulose-purified U-mRNA or m1Ψ-mRNA, using TransIT-mRNA Transfection Kit (Mirus Bio) according to manufacturer's instructions. Twenty-four h post transfection, supernatants were removed, monolayers washed twice with phosphate buffered saline (PBS), and cells collected either for flow cytometry or RNA extraction. All experiments were performed in biological triplicates.

Flow cytometry. Cells transfected with ANDV U-mRNA or m1Ψ-mRNA in 24-well plate format as described above were digested in 0.25 ml of 0.25% trypsin-EDTA (Gibco) which was further neutralized by an addition of 0.25 ml of calf serum (Corning). Cells were washed by PBS, fixed in 4% paraformaldehyde (Polysciences, Inc), and subjected to immunostaining with a cocktail of human monoclonal antibodies ANDV-4, -5, -12, -22, -23, -34, and – 44 targeting ANDV Gn/Gc and capable to both bind and neutralize the virus [10] diluted to 2 µg/ml in StartingBlock T 20 (TBS) Blocking Buffer (Thermo Scientific). After incubation during 1 h at room temperature and two PBS washes, cells were incubated with the secondary goat anti-human FITC-conjugated antibody (Southern Biotech) diluted 1:500 in TBS and incubated at the same conditions in the dark. Stained cells were double-washed in PBS and subjected to flow cytometry on Accuri C6 (BD Biosciences). The results were evaluated with FlowJo, version 10.8.

qRT-PCR for cytokine expression. A549 cells transfected with ANDV U-mRNA or m1Ψ-mRNA in 24-well plate format as described above were digested in 1.0 ml of TRIZol reagent (Invitrogen). After chloroform separation, aqueous phase was mixed with equal volume of 100% ethanol and processed with Direct-zol RNA MicroPrep (Zymo Research) with on-column DNAse I treatment. The extracted RNA was quantified using NanoDrop and reverse transcribed with High-Capacity cDNA Reverse Transcription Kit with RNase Inhibitor (Applied Biosystems) according to manufacturer's instructions. The resulting cDNA was diluted to 4–5 ng/µl, and PCR-amplified in the plates of TaqMan™ Array, Human Cytokine Network, Fast 96-well (Applied Biosystems) using TaqMan® Fast Advanced Master Mix (Applied Biosystems), on QuantStudio™ 6 Flex Real-Time PCR System (Applied Biosystems). Results of qRT-PCR were normalized on the expression values of GAPDH or 18S housekeeping genes, and quantified by ΔΔCt method [86].

Electron microscopy. 293T cells were transfected with 5 µg of ANDV mRNA in 6-well plates as described above. Forty-eight h post transfection, supernatant was collected into conical tubes, clarified by centrifugation at 12 x g for 10 min, filtered through Millex®-HP 0.45 µm syringe filter (Millipore Sigma) and concentrated 250x by ultracentrifugation at 100,000 x g for 2 h. Supernatant from 293T cells with added transfection reagents but without mRNA was used as negative control. The samples were incubated on copper grids, counterstained with 2% aqueous uranyl acetate, and observed at JEM-1400 electron microscope (JEOL Ltd), accelerating voltage 80 kV. To confirm specificity of the observed structures, samples were absorbed to nickel grids and immunostained with primary anti-ANDV human monoclonal antibodies (described above) and secondary 6 nm colloidal gold AffiniPure goat anti-human IgG (H + L) antibody (Jackson ImmunoResearch Laboratories, Inc) following post-staining fixation in 2% glutaraldehyde and counterstaining with 2% aqueous uranyl acetate.

Analysis of germinal centers in lymph nodes of immunized mice. Animal experimentation described in this manuscript was approved by the Institutional Animal Care and Use Committee (IACUC) of the University of Texas Medical Branch at Galveston. For analysis of germinal center phenotypes in mice, 10–12 week old female C57Bl6/J mice were immunized intramuscularly with one dose (5 µg) of either U-mRNA or m1Ψ-mRNA formulated with LNP. Positive control constituted 20 µg of recombinant Gn^H/Gc antigen formulated with Alhydrogel (2%) in a 1:1 ratio (total volume 50 µl). Inguinal and popliteal lymph nodes were pooled for each mouse on indicated day. Cells were counted, Fc blocked, and stained with indicated monoclonal antibodies that were commercially sourced (Biolegend and Beckton Dickenson). Key antibody clones used were: 11-26c.a2 (IgD), 281-2 (CD138), RA3-6B2 (B220), GL7 (GL7), 90 (CD38), GK1.5 (CD4), 53 – 6.7 (CD8). Cells were acquired on a BD LSR Fortessa and data analyzed using Flowjo v10.

Preparation of B cells from lymph nodes of immunized mice for single cell sequencing. Ten-week-old BALB/c mice, four per group, were immunized intramuscularly with one dose of 25 µg of either U-mRNA or m1Ψ-mRNA formulated with LNP. Positive control constituted 20 µg of recombinant Gn^H/Gc antigen formulated with Alhydrogel (2%) in a 1:1 ratio (total volume 50 µl), and negative control constituted a suspension of empty LNP in approximately the same concentration that was used in mRNA vaccines. In this experiment, lymph node drainage of the vaccine was noted bilaterally. Twelve days after

immunization animals were euthanized, and draining inguinal and popliteal lymph nodes harvested and pooled for each mouse for cell sorting.

Germinal center B cells were gated as single live lymphocytes that are B220+, CD4-, CD8-, GL7+, CD38-, IgD, CD138- and purified by cell sorting using the BD FACSaria Fusion sorter (Beckton Dickinson, Inc). For negative control, no sorting was performed due to the limited amount of germinal center B cells induced by the empty LNP vaccination. From this group, total lymphocytes were taken for sequencing.

B cell suspensions were processed for single cell sequencing following Chromium Next GEM Single Cell 5' Version 2 protocol. A pool of 750,000 barcodes were sampled individually to index the transcriptome of each cell. This was reached by partitioning each cell into Gel beads-in-emulsion (GEMs) combined with a Master Mix containing reverse transcription (RT) reagents and poly(dT) RT primers. The emulsion was made using the Chromium Controller device and Next GEM Chips (10x genomics). The GEM generation and further RT reaction produced 10x Barcoded full-length cDNA from poly-adenylated mRNA. This initial cDNA was PCR amplified to generate enough material for 5' Gene expression and BCR sequencing. Right after PCR amplification, bioanalyzer Quality Control (QC) was performed for all the samples using the Agilent Bioanalyzer High Sensitivity DNA assay in the 2100 expert software (Agilent). All the samples passed the initial QC with a cDNA size between 700–1500 bp.

Amplified full-length cDNA from poly-adenylated mRNA was used to generate 5' gene expression (GEX) and V(D)J libraries (BCR). For GEX library construction, the cDNA was enzymatically fragmented, and size selected to optimize the cDNA amplicon size. For V(D)J library construction, full-length cDNA was used to amplify 10X barcoded V(D)J segments by PCR amplification using specific primers for BCR constant regions. BCR transcripts were fragmented and selected to get variable length fragments that span the V(D)J segments. P5, P7, i5 and i7 sample indexes, and Illumina R2 sequence (read 2 primer sequence) were added via End Repair, A-tailing, Adaptor ligation and sample index PCR for both GEX and BCR libraries. A second Quality Control was performed for each type of library before sequencing. The electropherograms showed a library size between 500 to 900 bp, the size expected for the GEX constructs, and 600 bp for BCR libraries. Finally, libraries were pooled and sequenced by the New York Genome Center (NYGC) using a NovaSeq sequencer and S2 and SP flow-cell for GEX and BCR libraries respectively.

Processing of Single-Cell Sequencing Data. The output FASTA files from single cell GEX RNA-sequencing (scRNA-seq) and single cell BCR-sequencing (scBCR-seq) were processed using Cell Ranger 7.1 (10X Genomics) as described elsewhere [87]. The Cell Ranger *counts* pipeline was used for scRNA-seq data, and the Cell Ranger *vdj* pipeline was used to process scBCR-seq data. For the scRNA-seq pipeline, the vaccine RNA sequence was added to the GRCm38 mouse reference genome prior to alignment. The aligned sequences for gene expression and BCR were then processed in Python using Scanpy 1.9.1 [88] and custom scripts. Only barcodes for cells detected in both the scRNA-seq and scBCR-seq data were retained for downstream analyses.

scRNA-seq Pipeline

Preprocessing

Following alignment of the mRNA reads to the reference genome, the scRNA-seq data was processed in Scanpy. Cells with less than 5000 total gene counts or a total percentage of reads from mitochondrial genes > 5% were removed in order to filter out poor quality and lysed cells. Reads were log-normalized with a scale factor of 10^4 within each sample and then scaled to unit variance and zero mean. Genes encoding for V(D)J regions of the IGH, IGK, and IGL loci were removed, and then the gene expression matrices from all samples were concatenated prior to clustering. Highly Variable Genes (HVG) with minimum dispersion of 0.5 were selected for use in dimensionality reduction and clustering.

Dimensionality Reduction and Clustering

Dimensionality reduction and clustering was performed based on the recommended clustering pipeline provided in the Scanpy documentation. Principal Component Analysis (PCA) was used to reduce the gene expression matrix to the first 30 principal components, which were then used to construct a nearest neighbor graph with k = 20. Uniform Manifold Approximation Projection (UMAP) was used to obtain a two-dimensional representation of the data for downstream analyses and visualization, followed by unsupervised clustering using the Scanpy implementation of the Leiden algorithm [89] with a resolution of 0.5.

Further Gene Expression Analysis

Only IgG-expressing B cells were retained for further analysis, as these B cells are expected to be elicited by the vaccine treatments, and differences in gene expression between B cell subtypes could convolute the downstream analyses. Differential gene expression (DGE) analysis was performed to identify differentially expressed genes between the cells from mice in the U-mRNA and m1Ψ-mRNA groups based on Benjamini-Hochberg adjusted p-values. DGE was also performed between Cluster 9 cells and the rest of the matrix to identify upregulated genes in this cluster (Fig. S2).

Gene Set Enrichment Analysis

The Python library GSEAPY [90] was used to perform Gene Set Enrichment Analysis (GSEA) based on their recommended scRNA-seq workflow to identify enrichment of gene sets from the *GO Biological Processes 2021* database [91]. GSEA was performed on the significant differential genes from Cluster 9 in comparison to all other cells. Only differentially expressed genes with a log fold change > 0 and an adjusted p-value < 0.05 were used to identify upregulated gene sets.

BCR analysis. The BCR contigs obtained from the Cell Ranger *vdj* pipeline were aligned to the IMGT mouse reference database using IMGT/High-V Quest [92]. These aligned sequences were further analyzed using a custom Python script to visualize differences in CDRH-3 length, identity, and heavy chain isotype.

Testing of the protective efficacy of ANDV mRNA constructs in golden Syrian hamster model. Golden Syrian hamsters, 10-weeks old, five animals per group, were immunized twice intramuscularly (gastrocnemius muscle) with 25 µg of LNP-encapsulated vaccines, either U-mRNA or m1Ψ-mRNA, with an interval of 21 days. Twenty-one days after the second immunization, the animals were transferred to the BSL-4 facility of the Galveston National Laboratory and challenged intramuscularly with 250 PFU of ANDV. The animals were observed until 28 days post challenge. If clinical signs were detected, hamsters were observed more frequently and euthanized based on disease scores. Blood serum was collected from hamsters on days 0 (baseline), 21 (pre-boost), 41 (pre-challenge), 56 (14 days post challenge), and at euthanasia (terminal). Liver and lung tissue samples were collected at necropsy.

ELISA for anti-Gn/Gc and anti-N IgG. Reactions were performed as described elsewhere [22] using Falcon™ 96-Well Non-Treated Flat-Bottom Microplates (Corning). Recombinant ANDV Gn^{H}/Gc antigen [8] and recombinant Puumala virus N antigen [72] which was demonstrated previously to cross-react with ANDV N protein [24] were used as antigens to cover the microplates. Serum samples were tested in 2-fold dilutions starting from 1:100, in duplicates. The secondary antibody was HRP-conjugated goat anti-hamster IgG (H + L) Cross Adsorbed (Invitrogen) in dilution 1:1500 as determined by checkerboard titration. After incubation with 1-Step Ultra TMB-ELISA (Thermo Scientific) in the dark for 10–15 min, the reactions were terminated by the addition of 1N sulfuric acid and detected on Synergy HT Microplate Reader (Bio Tek) at 450 nm. A pool of 10 serum samples from golden Syrian hamsters never exposed to hantaviruses was used as a negative control, whereas a pool of five serum samples from golden Syrian hamsters that survived challenge with ANDV in previous experiments was used as a positive control.

Detection of ANDV- and SNV-neutralizing antibodies. The plaque reduction-neutralization test was performed with hamster sera in 96-well format. Serum samples were inactivated at 56 ^{o}C for 30 min, and 2-fold dilutions in MEM with 10% guinea pig complement (MP Biologicals) were mixed with approximately 50 PFU of ANDV or SNV, starting from serum dilution 1:10 (final dilution 1:20 after mixing with virus). The mixtures were incubated at 37 ^{o}C for 1 h and placed on monolayer of Vero cells. After 1 h incubation the inocula were removed, and MEM with 10% FBS and 0.5% methylcellulose overlay was added onto cells. The plates were incubated for 6 days, then fixed in 10% buffered formalin and removed from BSL-4 biocontainment for immunostaining. The immunostaining was performed with a mixture of human monoclonal antibodies as described above (see flow cytometry section), and secondary HRP-conjugated goat anti-human antibody (SeraCare). The reactions were visualized with ImmPACT AEC Substrate (Vector Laboratories). The plates were observed under CKX53 inverted microscope (Olympus) at 10^{x} magnification, and 50% inhibitory concentrations (IC50) of serum samples were determined.

Statistical statement. All statistical analysis were performed with GraphPad Prism, version 9.5.0. Unless stated otherwise, results were expressed as mean ± SD, and 95% confidence interval (CI_{95}) was calculated where applicable. Unpaired two-sided T-test was used to assess statistical differences between animal group samples or biological triplicates in in-vitro experiments. Non-parametric unpaired Kruskal-Wallis test was used when multiple groups were being compared. The Yates corrected chi-

square and Fisher's exact tests were used for comparison of survival rates in groups of experimental animals.

Declarations

ACKNOWLEDGEMENTS

We thank Dr. Jay Hooper (USAMRIID, Frederick, MD, USA) for providing the recombinant Puumala virus nucleoprotein antigen used for N-IgG ELISA, and Keziah Hernandez for assistance with preparing the figures. This project was funded by UTMB intramural funds. Figures 2A, 3A and 6A were created with BioRender.

References

1. Kuhn, J. H. *et al.* 2021 Taxonomic update of phylum Negarnaviricota (Riboviria: Orthornavirae), including the large orders Bunyavirales and Mononegavirales. *Arch Virol* **166**, 3513-3566, doi:10.1007/s00705-021-05143-6 (2021).
2. Macneil, A., Nichol, S. T. & Spiropoulou, C. F. Hantavirus pulmonary syndrome. *Virus Res* **162**, 138-147, doi:10.1016/j.virusres.2011.09.017 (2011).
3. Kruger, D. H., Figueiredo, L. T., Song, J. W. & Klempa, B. Hantaviruses--globally emerging pathogens. *J Clin Virol* **64**, 128-136, doi:10.1016/j.jcv.2014.08.033 (2015).
4. Goodfellow, S. M. *et al.* Tracing Transmission of Sin Nombre Virus and Discovery of Infection in Multiple Rodent Species. *J Virol* **95**, e0153421, doi:10.1128/JVI.01534-21 (2021).
5. Schmaljohn, C. S. & Dalrymple, J. M. Analysis of Hantaan virus RNA: evidence for a new genus of bunyaviridae. *Virology* **131**, 482-491, doi:10.1016/0042-6822(83)90514-7 (1983).
6. Spiropoulou, C. F. *et al.* Genome structure and variability of a virus causing hantavirus pulmonary syndrome. *Virology* **200**, 715-723, doi:10.1006/viro.1994.1235 (1994).
7. Lober, C., Anheier, B., Lindow, S., Klenk, H. D. & Feldmann, H. The Hantaan virus glycoprotein precursor is cleaved at the conserved pentapeptide WAASA. *Virology* **289**, 224-229, doi:10.1006/viro.2001.1171 (2001).
8. Serris, A. *et al.* The Hantavirus Surface Glycoprotein Lattice and Its Fusion Control Mechanism. *Cell* **183**, 442-456 e416, doi:10.1016/j.cell.2020.08.023 (2020).
9. Guardado-Calvo, P. & Rey, F. A. The surface glycoproteins of hantaviruses. *Curr Opin Virol* **50**, 87-94, doi:10.1016/j.coviro.2021.07.009 (2021).
10. Engdahl, T. B. *et al.* Broad and potently neutralizing monoclonal antibodies isolated from human survivors of New World hantavirus infection. *Cell Rep* **36**, 109453, doi:10.1016/j.celrep.2021.109453 (2021).
11. Hooper, J. W. & Li, D. Vaccines against hantaviruses. *Curr Top Microbiol Immunol* **256**, 171-191, doi:10.1007/978-3-642-56753-7_10 (2001).

12. Ronnberg, B. *et al.* Serogrouping and seroepidemiology of North European hantaviruses using a novel broadly targeted synthetic nucleoprotein antigen array. *Infect Ecol Epidemiol* **7**, 1350086, doi:10.1080/20008686.2017.1350086 (2017).
13. Hooper, J. W., Custer, D. M., Smith, J. & Wahl-Jensen, V. Hantaan/Andes virus DNA vaccine elicits a broadly cross-reactive neutralizing antibody response in nonhuman primates. *Virology* **347**, 208-216, doi:10.1016/j.virol.2005.11.035 (2006).
14. Custer, D. M., Thompson, E., Schmaljohn, C. S., Ksiazek, T. G. & Hooper, J. W. Active and passive vaccination against hantavirus pulmonary syndrome with Andes virus M genome segment-based DNA vaccine. *J Virol* **77**, 9894-9905, doi:10.1128/jvi.77.18.9894-9905.2003 (2003).
15. Chu, Y. K., Jennings, G. B. & Schmaljohn, C. S. A vaccinia virus-vectored Hantaan virus vaccine protects hamsters from challenge with Hantaan and Seoul viruses but not Puumala virus. *J Virol* **69**, 6417-6423, doi:10.1128/JVI.69.10.6417-6423.1995 (1995).
16. Schmaljohn, C. S. Vaccines for hantaviruses: progress and issues. *Expert Rev Vaccines* **11**, 511-513, doi:10.1586/erv.12.15 (2012).
17. Liu, R. *et al.* Vaccines and Therapeutics Against Hantaviruses. *Frontiers in microbiology* **10**, 2989, doi:10.3389/fmicb.2019.02989 (2019).
18. Warner, B. M. *et al.* Vesicular Stomatitis Virus-Based Vaccines Provide Cross-Protection against Andes and Sin Nombre Viruses. *Viruses* **11**, doi:10.3390/v11070645 (2019).
19. Brown, K. S., Safronetz, D., Marzi, A., Ebihara, H. & Feldmann, H. Vesicular stomatitis virus-based vaccine protects hamsters against lethal challenge with Andes virus. *J Virol* **85**, 12781-12791, doi:10.1128/JVI.00794-11 (2011).
20. Prescott, J., DeBuysscher, B. L., Brown, K. S. & Feldmann, H. Long-term single-dose efficacy of a vesicular stomatitis virus-based Andes virus vaccine in Syrian hamsters. *Viruses* **6**, 516-523, doi:10.3390/v6020516 (2014).
21. Safronetz, D. *et al.* Adenovirus vectors expressing hantavirus proteins protect hamsters against lethal challenge with andes virus. *J Virol* **83**, 7285-7295, doi:10.1128/JVI.00373-09 (2009).
22. Hooper, J. W., Kamrud, K. I., Elgh, F., Custer, D. & Schmaljohn, C. S. DNA vaccination with hantavirus M segment elicits neutralizing antibodies and protects against seoul virus infection. *Virology* **255**, 269-278, doi:10.1006/viro.1998.9586 (1999).
23. Hooper, J. W., Custer, D. M., Thompson, E. & Schmaljohn, C. S. DNA vaccination with the Hantaan virus M gene protects Hamsters against three of four HFRS hantaviruses and elicits a high-titer neutralizing antibody response in Rhesus monkeys. *J Virol* **75**, 8469-8477, doi:10.1128/jvi.75.18.8469-8477.2001 (2001).
24. Brocato, R. L., Josleyn, M. J., Wahl-Jensen, V., Schmaljohn, C. S. & Hooper, J. W. Construction and nonclinical testing of a Puumala virus synthetic M gene-based DNA vaccine. *Clin Vaccine Immunol* **20**, 218-226, doi:10.1128/CVI.00546-12 (2013).
25. Hooper, J. *et al.* A Phase 2a Randomized, Double-Blind, Dose-Optimizing Study to Evaluate the Immunogenicity and Safety of a Bivalent DNA Vaccine for Hemorrhagic Fever with Renal Syndrome

Delivered by Intramuscular Electroporation. *Vaccines (Basel)* **8**, doi:10.3390/vaccines8030377 (2020).

26. Hooper, J. W. *et al.* DNA vaccine-derived human IgG produced in transchromosomal bovines protect in lethal models of hantavirus pulmonary syndrome. *Sci Transl Med* **6**, 264ra162, doi:10.1126/scitranslmed.3010082 (2014).
27. Boudreau, E. F. *et al.* A Phase 1 clinical trial of Hantaan virus and Puumala virus M-segment DNA vaccines for hemorrhagic fever with renal syndrome. *Vaccine* **30**, 1951-1958, doi:10.1016/j.vaccine.2012.01.024 (2012).
28. Pardi, N., Hogan, M. J., Porter, F. W. & Weissman, D. mRNA vaccines - a new era in vaccinology. *Nat Rev Drug Discov* **17**, 261-279, doi:10.1038/nrd.2017.243 (2018).
29. Pardi, N. *et al.* Nucleoside-modified mRNA vaccines induce potent T follicular helper and germinal center B cell responses. *J Exp Med* **215**, 1571-1588, doi:10.1084/jem.20171450 (2018).
30. Pardi, N., Hogan, M. J. & Weissman, D. Recent advances in mRNA vaccine technology. *Curr Opin Immunol* **65**, 14-20, doi:10.1016/j.coi.2020.01.008 (2020).
31. Laczko, D. *et al.* A Single Immunization with Nucleoside-Modified mRNA Vaccines Elicits Strong Cellular and Humoral Immune Responses against SARS-CoV-2 in Mice. *Immunity* **53**, 724-732 e727, doi:10.1016/j.immuni.2020.07.019 (2020).
32. Elkhalifa, D., Rayan, M., Negmeldin, A. T., Elhissi, A. & Khalil, A. Chemically modified mRNA beyond COVID-19: Potential preventive and therapeutic applications for targeting chronic diseases. *Biomed Pharmacother* **145**, 112385, doi:10.1016/j.biopha.2021.112385 (2022).
33. Kon, E., Elia, U. & Peer, D. Principles for designing an optimal mRNA lipid nanoparticle vaccine. *Curr Opin Biotechnol* **73**, 329-336, doi:10.1016/j.copbio.2021.09.016 (2021).
34. Hogan, M. J. & Pardi, N. mRNA Vaccines in the COVID-19 Pandemic and Beyond. *Annu Rev Med* **73**, 17-39, doi:10.1146/annurev-med-042420-112725 (2022).
35. Pollard, C., De Koker, S., Saelens, X., Vanham, G. & Grooten, J. Challenges and advances towards the rational design of mRNA vaccines. *Trends in Molecular Medicine* **19**, 705-713, doi:https://doi.org/10.1016/j.molmed.2013.09.002 (2013).
36. Alameh, M. G. *et al.* Lipid nanoparticles enhance the efficacy of mRNA and protein subunit vaccines by inducing robust T follicular helper cell and humoral responses. *Immunity* **54**, 2877-2892 e2877, doi:10.1016/j.immuni.2021.11.001 (2021).
37. Kariko, K., Buckstein, M., Ni, H. & Weissman, D. Suppression of RNA recognition by Toll-like receptors: the impact of nucleoside modification and the evolutionary origin of RNA. *Immunity* **23**, 165-175, doi:10.1016/j.immuni.2005.06.008 (2005).
38. Anderson, B. R. *et al.* Incorporation of pseudouridine into mRNA enhances translation by diminishing PKR activation. *Nucleic Acids Res* **38**, 5884-5892, doi:10.1093/nar/gkq347 (2010).
39. Andries, O. *et al.* N(1)-methylpseudouridine-incorporated mRNA outperforms pseudouridine-incorporated mRNA by providing enhanced protein expression and reduced immunogenicity in

mammalian cell lines and mice. *J Control Release* **217**, 337-344, doi:10.1016/j.jconrel.2015.08.051 (2015).

40. Kariko, K. *et al.* Incorporation of pseudouridine into mRNA yields superior nonimmunogenic vector with increased translational capacity and biological stability. *Mol Ther* **16**, 1833-1840, doi:10.1038/mt.2008.200 (2008).
41. Verbeke, R., Hogan, M. J., Lore, K. & Pardi, N. Innate immune mechanisms of mRNA vaccines. *Immunity* **55**, 1993-2005, doi:10.1016/j.immuni.2022.10.014 (2022).
42. Mu, X., Greenwald, E., Ahmad, S. & Hur, S. An origin of the immunogenicity of in vitro transcribed RNA. *Nucleic Acids Res* **46**, 5239-5249, doi:10.1093/nar/gky177 (2018).
43. Kremsner, P. G. *et al.* Efficacy and safety of the CVnCoV SARS-CoV-2 mRNA vaccine candidate in ten countries in Europe and Latin America (HERALD): a randomised, observer-blinded, placebo-controlled, phase 2b/3 trial. *Lancet Infect Dis* **22**, 329-340, doi:10.1016/S1473-3099(21)00677-0 (2022).
44. Gebre, M. S. *et al.* Optimization of non-coding regions for a non-modified mRNA COVID-19 vaccine. *Nature* **601**, 410-414, doi:10.1038/s41586-021-04231-6 (2022).
45. Medina-Magues, L. G. *et al.* Immunogenicity and protective activity of mRNA vaccine candidates against yellow fever virus in animal models. *NPJ Vaccines* **8**, 31, doi:10.1038/s41541-023-00629-7 (2023).
46. Pulendran, B., P, S. A. & O'Hagan, D. T. Emerging concepts in the science of vaccine adjuvants. *Nat Rev Drug Discov* **20**, 454-475, doi:10.1038/s41573-021-00163-y (2021).
47. Le Bon, A. *et al.* Type i interferons potently enhance humoral immunity and can promote isotype switching by stimulating dendritic cells in vivo. *Immunity* **14**, 461-470, doi:10.1016/s1074-7613(01)00126-1 (2001).
48. Gujer, C. *et al.* IFN-α produced by human plasmacytoid dendritic cells enhances T cell-dependent naïve B cell differentiation. *Journal of leukocyte biology* **89**, 811-821, doi:10.1189/jlb.0810460 (2011).
49. Martinez, V. P. *et al.* "Super-Spreaders" and Person-to-Person Transmission of Andes Virus in Argentina. *N Engl J Med* **383**, 2230-2241, doi:10.1056/NEJMoa2009040 (2020).
50. Hernandez, G., Osnaya, V. G. & Perez-Martinez, X. Conservation and Variability of the AUG Initiation Codon Context in Eukaryotes. *Trends Biochem Sci* **44**, 1009-1021, doi:10.1016/j.tibs.2019.07.001 (2019).
51. Orlandini von Niessen, A. G. *et al.* Improving mRNA-Based Therapeutic Gene Delivery by Expression-Augmenting 3' UTRs Identified by Cellular Library Screening. *Mol Ther* **27**, 824-836, doi:10.1016/j.ymthe.2018.12.011 (2019).
52. Baiersdorfer, M. *et al.* A Facile Method for the Removal of dsRNA Contaminant from In Vitro-Transcribed mRNA. *Mol Ther Nucleic Acids* **15**, 26-35, doi:10.1016/j.omtn.2019.02.018 (2019).
53. Overby, A. K., Popov, V., Neve, E. P. & Pettersson, R. F. Generation and analysis of infectious virus-like particles of uukuniemi virus (bunyaviridae): a useful system for studying bunyaviral packaging and

budding. *J Virol* **80**, 10428-10435, doi:10.1128/JVI.01362-06 (2006).

54. Acuna, R. *et al.* Hantavirus Gn and Gc glycoproteins self-assemble into virus-like particles. *J Virol* **88**, 2344-2348, doi:10.1128/JVI.03118-13 (2014).
55. Lee, H. W. & Cho, H. J. Electron microscope appearance of Hantaan virus, the causative agent of Korean haemorrhagic fever. *Lancet* **1**, 1070-1072, doi:10.1016/s0140-6736(81)92240-6 (1981).
56. Martin, M. L., Lindsey-Regnery, H., Sasso, D. R., McCormick, J. B. & Palmer, E. Distinction between Bunyaviridae genera by surface structure and comparison with Hantaan virus using negative stain electron microscopy. *Arch Virol* **86**, 17-28, doi:10.1007/BF01314110 (1985).
57. White, J. D. *et al.* Hantaan virus, aetiological agent of Korean haemorrhagic fever, has Bunyaviridae-like morphology. *Lancet* **1**, 768-771, doi:10.1016/s0140-6736(82)91813-x (1982).
58. Huiskonen, J. T. *et al.* Electron cryotomography of Tula hantavirus suggests a unique assembly paradigm for enveloped viruses. *J Virol* **84**, 4889-4897, doi:10.1128/JVI.00057-10 (2010).
59. Battisti, A. J. *et al.* Structural studies of Hantaan virus. *J Virol* **85**, 835-841, doi:10.1128/JVI.01847-10 (2011).
60. Plotkin, S. A. Correlates of protection induced by vaccination. *Clin Vaccine Immunol* **17**, 1055-1065, doi:10.1128/cvi.00131-10 (2010).
61. Bannard, O. & Cyster, J. G. Germinal centers: programmed for affinity maturation and antibody diversification. *Curr Opin Immunol* **45**, 21-30, doi:10.1016/j.coi.2016.12.004 (2017).
62. Eisen, H. N. Affinity enhancement of antibodies: how low-affinity antibodies produced early in immune responses are followed by high-affinity antibodies later and in memory B-cell responses. *Cancer immunology research* **2**, 381-392, doi:10.1158/2326-6066.cir-14-0029 (2014).
63. Montoya, M. *et al.* Type I interferons produced by dendritic cells promote their phenotypic and functional activation. *Blood* **99**, 3263-3271, doi:10.1182/blood.v99.9.3263 (2002).
64. Seo, Y. J. & Hahm, B. Type I interferon modulates the battle of host immune system against viruses. *Adv Appl Microbiol* **73**, 83-101, doi:10.1016/S0065-2164(10)73004-5 (2010).
65. Petrović, R. *et al.* Mouse strain and sex as determinants of immune response to trivalent influenza vaccine. *Life sciences* **207**, 117-126, doi:10.1016/j.lfs.2018.05.056 (2018).
66. Chen, R. *et al.* Engineering circular RNA for enhanced protein production. *Nat Biotechnol*, doi:10.1038/s41587-022-01393-0 (2022).
67. Wesselhoeft, R. A. *et al.* RNA Circularization Diminishes Immunogenicity and Can Extend Translation Duration In Vivo. *Mol Cell* **74**, 508-520 e504, doi:10.1016/j.molcel.2019.02.015 (2019).
68. Röltgen, K. *et al.* Immune imprinting, breadth of variant recognition, and germinal center response in human SARS-CoV-2 infection and vaccination. *Cell* **185**, 1025-1040.e1014, doi:10.1016/j.cell.2022.01.018 (2022).
69. Cirelli, K. M. *et al.* Slow Delivery Immunization Enhances HIV Neutralizing Antibody and Germinal Center Responses via Modulation of Immunodominance. *Cell* **177**, 1153-1171.e1128, doi:10.1016/j.cell.2019.04.012 (2019).

70. Tam, H. H. *et al.* Sustained antigen availability during germinal center initiation enhances antibody responses to vaccination. *Proceedings of the National Academy of Sciences of the United States of America* **113**, E6639-e6648, doi:10.1073/pnas.1606050113 (2016).
71. Engdahl, T. B. *et al.* Antigenic mapping and functional characterization of human new world hantavirus neutralizing antibodies. *Elife* **12**, doi:10.7554/eLife.81743 (2023).
72. Elgh, F. *et al.* Serological diagnosis of hantavirus infections by an enzyme-linked immunosorbent assay based on detection of immunoglobulin G and M responses to recombinant nucleocapsid proteins of five viral serotypes. *J Clin Microbiol* **35**, 1122-1130, doi:10.1128/jcm.35.5.1122-1130.1997 (1997).
73. Pardi, N. *et al.* Zika virus protection by a single low-dose nucleoside-modified mRNA vaccination. *Nature* **543**, 248-251, doi:10.1038/nature21428 (2017).
74. Pardi, N. *et al.* Nucleoside-modified mRNA immunization elicits influenza virus hemagglutinin stalk-specific antibodies. *Nat Commun* **9**, 3361, doi:10.1038/s41467-018-05482-0 (2018).
75. Petsch, B. *et al.* Protective efficacy of in vitro synthesized, specific mRNA vaccines against influenza A virus infection. *Nat Biotechnol* **30**, 1210-1216, doi:10.1038/nbt.2436 (2012).
76. Schnee, M. *et al.* An mRNA Vaccine Encoding Rabies Virus Glycoprotein Induces Protection against Lethal Infection in Mice and Correlates of Protection in Adult and Newborn Pigs. *PLoS Negl Trop Dis* **10**, e0004746, doi:10.1371/journal.pntd.0004746 (2016).
77. Dolgin, E. CureVac COVID vaccine let-down spotlights mRNA design challenges. *Nature* **594**, 483, doi:10.1038/d41586-021-01661-0 (2021).
78. Hooper, J. W., Josleyn, M., Ballantyne, J. & Brocato, R. A novel Sin Nombre virus DNA vaccine and its inclusion in a candidate pan-hantavirus vaccine against hantavirus pulmonary syndrome (HPS) and hemorrhagic fever with renal syndrome (HFRS). *Vaccine* **31**, 4314-4321, doi:10.1016/j.vaccine.2013.07.025 (2013).
79. Xia, X. Detailed Dissection and Critical Evaluation of the Pfizer/BioNTech and Moderna mRNA Vaccines. *Vaccines (Basel)* **9**, doi:10.3390/vaccines9070734 (2021).
80. Kim, S. C. *et al.* Modifications of mRNA vaccine structural elements for improving mRNA stability and translation efficiency. *Mol Cell Toxicol* **18**, 1-8, doi:10.1007/s13273-021-00171-4 (2022).
81. Pardi, N. & Weissman, D. Development of vaccines and antivirals for combating viral pandemics. *Nat Biomed Eng* **4**, 1128-1133, doi:10.1038/s41551-020-00658-w (2020).
82. Hooper, J. W., Larsen, T., Custer, D. M. & Schmaljohn, C. S. A lethal disease model for hantavirus pulmonary syndrome. *Virology* **289**, 6-14, doi:10.1006/viro.2001.1133 (2001).
83. Tahtinen, S. *et al.* IL-1 and IL-1ra are key regulators of the inflammatory response to RNA vaccines. *Nat Immunol* **23**, 532-542, doi:10.1038/s41590-022-01160-y (2022).
84. Pardi, N., Muramatsu, H., Weissman, D. & Kariko, K. In vitro transcription of long RNA containing modified nucleosides. *Methods Mol Biol* **969**, 29-42, doi:10.1007/978-1-62703-260-5_2 (2013).

85. Walker, S. E. & Lorsch, J. RNA purification--precipitation methods. *Methods Enzymol* **530**, 337-343, doi:10.1016/B978-0-12-420037-1.00019-1 (2013).
86. Livak, K. J. & Schmittgen, T. D. Analysis of relative gene expression data using real-time quantitative PCR and the 2(-Delta Delta C(T)) Method. *Methods* **25**, 402-408, doi:10.1006/meth.2001.1262 (2001).
87. Zheng, G. X. *et al.* Massively parallel digital transcriptional profiling of single cells. *Nat Commun* **8**, 14049, doi:10.1038/ncomms14049 (2017).
88. Wolf, F. A., Angerer, P. & Theis, F. J. SCANPY: large-scale single-cell gene expression data analysis. *Genome Biol* **19**, 15, doi:10.1186/s13059-017-1382-0 (2018).
89. Traag, V. A., Waltman, L. & van Eck, N. J. From Louvain to Leiden: guaranteeing well-connected communities. *Sci Rep* **9**, 5233, doi:10.1038/s41598-019-41695-z (2019).
90. Fang, Z., Liu, X. & Peltz, G. GSEApy: a comprehensive package for performing gene set enrichment analysis in Python. *Bioinformatics* **39**, doi:10.1093/bioinformatics/btac757 (2023).
91. Consortium, G. O. The Gene Ontology resource: enriching a GOld mine. *Nucleic Acids Res* **49**, D325-D334, doi:10.1093/nar/gkaa1113 (2021).
92. Lefranc, M. P. *et al.* IMGT, the international ImMunoGeneTics information system. *Nucleic Acids Res* **37**, D1006-1012, doi:10.1093/nar/gkn838 (2009).

Figures

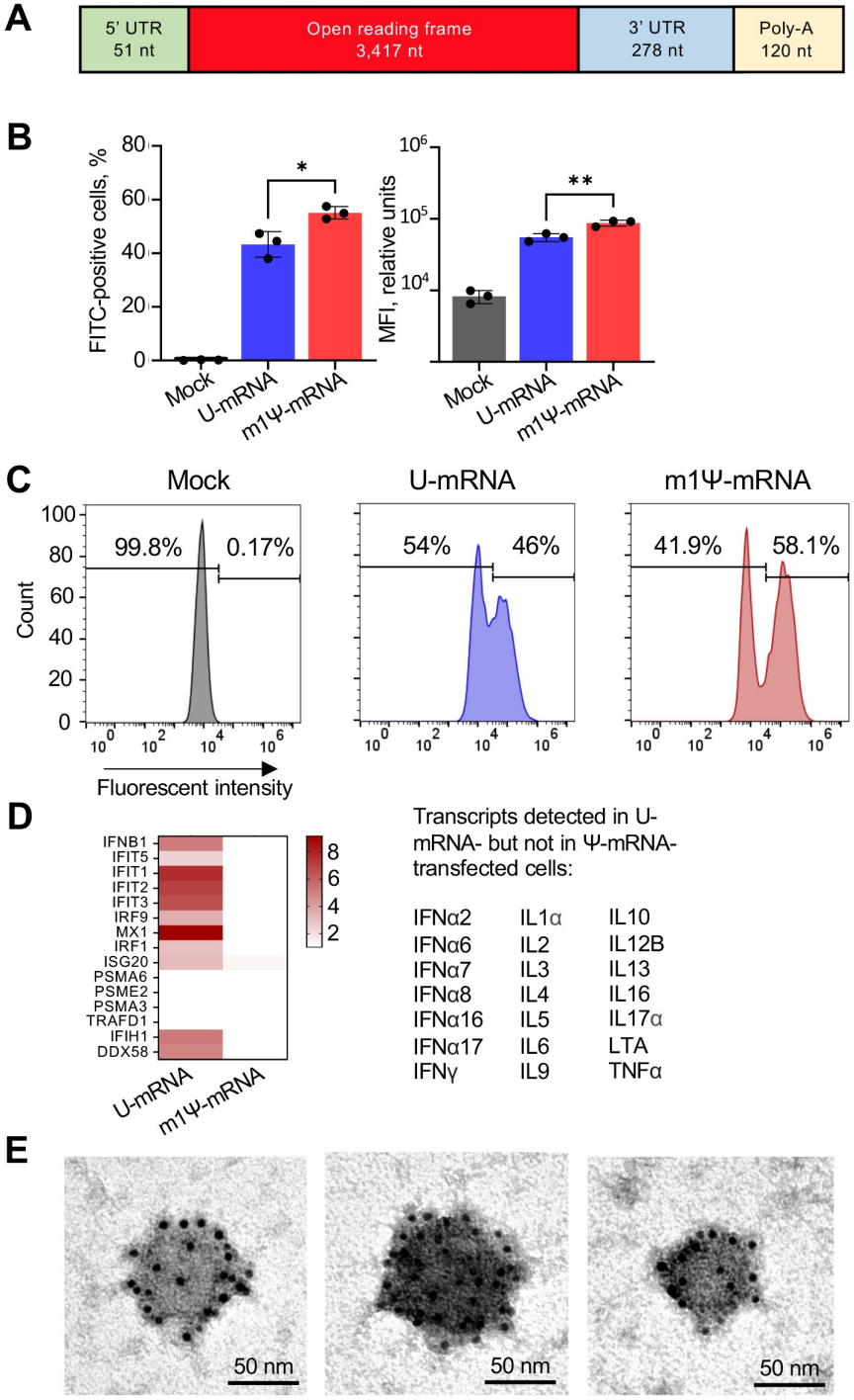

Figure 1

Generation of ANDV mRNA vaccine. A. Schematic representation of the vaccine construct. B, C. Expression of Gn/Gc evaluated by flow cytometry in A549 cells at 24 h post transfection with the RNA constructs: mean values ± SD,*p<0.05, **p<0.01, unpaired two-sided T-test (B) and primary data (C). D. Left: heatmap of cytokine expression in A549 cells at 24 h after transfection with the mRNA constructs, the scale bar shows log2 fold changes. Right: transcripts detected in U-mRNA-transfected, but not in

m1Ψ-mRNA-transfected cells. E. Electron microscopy of VLPs in supernatants of 293T cells transfected with ANDV U-mRNA. Immunostaining with a primary human ANDV antibody cocktail and secondary 6 nm colloidal gold anti-human antibody.

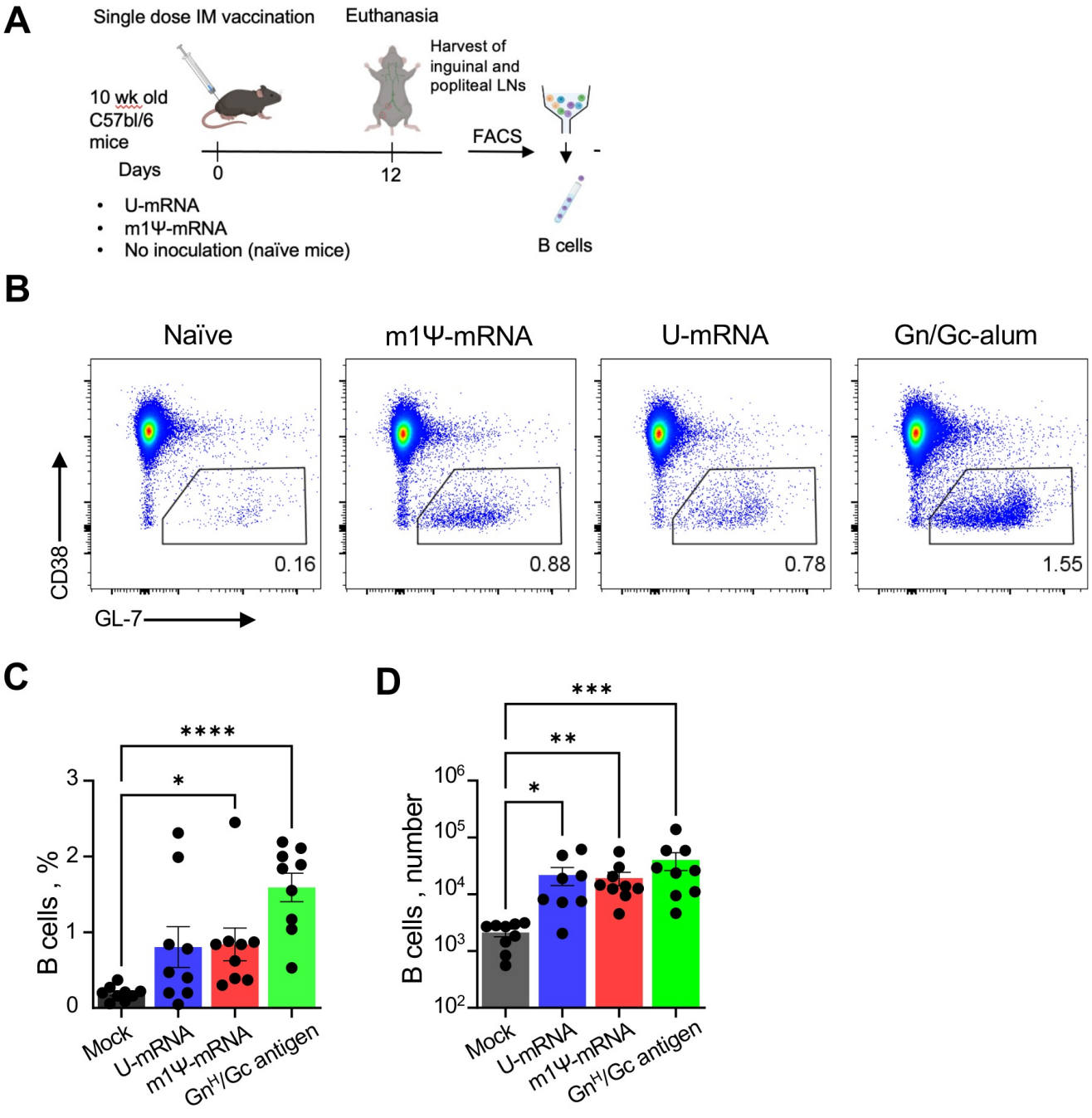

Figure 2

Single doses of ANDV U-mRNA and Ψ-mRNA induce comparable germinal center response in vaccinated mice. Female C57Bl6/J mice were immunized i.m. with a single 5 µg dose of the indicated ANDV mRNA vaccines or ANDV GnH/Gc-Alum antigen. Untreated age matched mice were used as naïve controls.

Twelve-days post vaccination, mice were euthanized and assessed for induction of GCs in pooled inguinal and popliteal draining lymph nodes. A. Representative flow cytometry plots of GCs from each group of mice. GC B cells were gated as scatter/singlet/live/B220+/dump-/CD38-/GL7+. B, C. Quantitation of GC B cell frequencies as indicated in A on day 12 post immunization. Data is pooled from two independent experiments; proportion (B) and absolute counts (C). * p <0.05, ** p <0.01, **** p <0.0001, unpaired Kruskal-Wallis test.

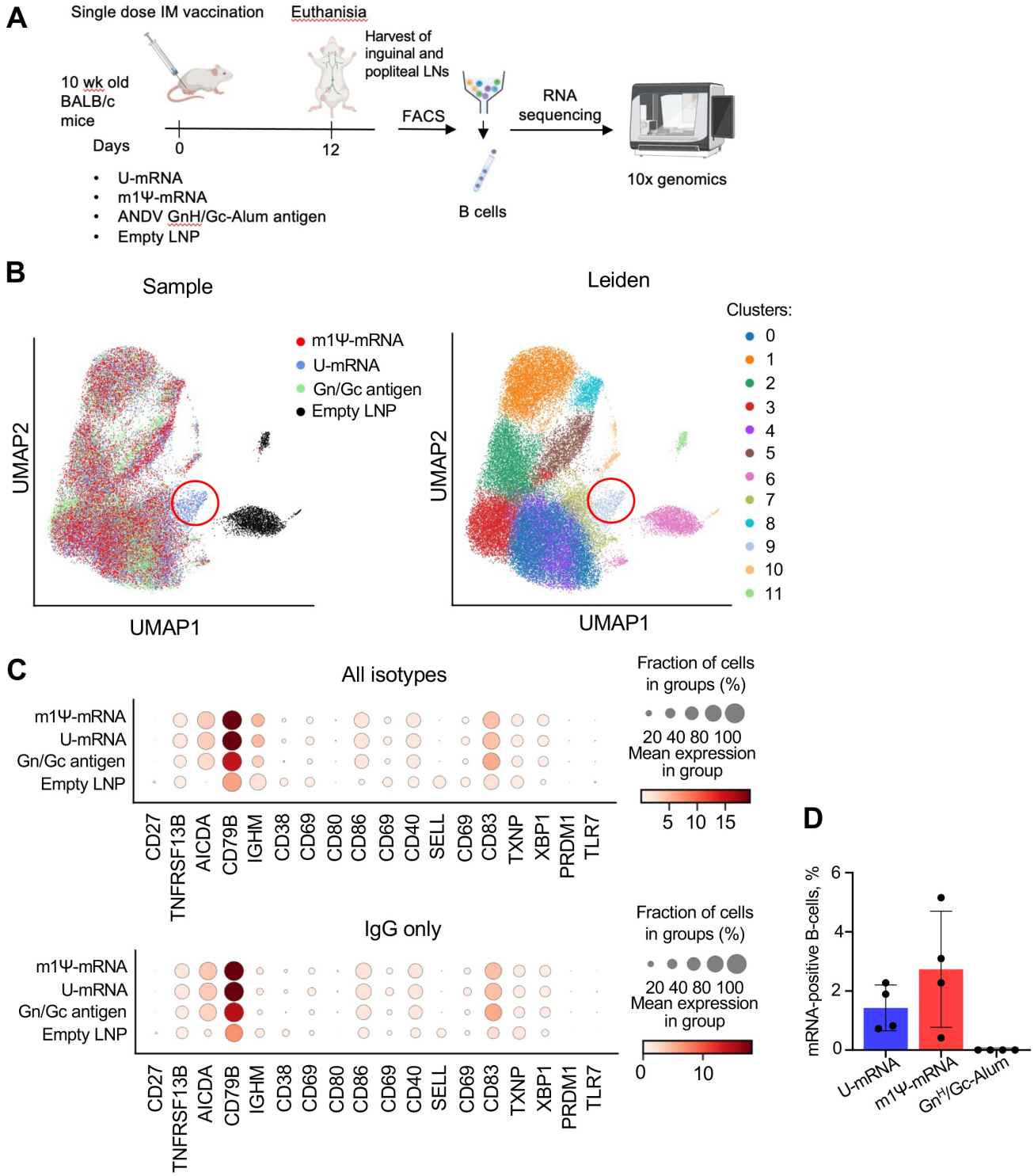

Figure 3

Single doses of ANDV U-mRNA and Ψ-mRNA induce similar gene expression patterns in vaccinated mice. A. Schematic representation of the experiment: BALB/c mice were immunized i.m. with single dose of ANDV mRNA vaccines, with ANDV GnH/Gc-Alum antigen, or with empty LNP. Twelve days post vaccination animals were euthanized, lymph nodes harvested, B cells were isolated and subjected to single-cell RNAseq and single cell sequencing of BCR (Fig. 5). B. Two-dimensional UMAP projection of B cell single-cell RNA-seq profiles across all vaccination groups. Unsupervised clustering of the B cells based on gene expression yielded 12 distinct clusters. Immunoglobulin genes were excluded before clustering. Cluster 9, which was present only in mice immunized with U-mRNA only is highlighted with a red circle. C. Mean expression of B cell activation and plasma cell markers across the groups. D. Vaccine-derived U-mRNA and Ψ-mRNA persist in lymph nodes B cells of mice for at least 12 days post vaccination. Vaccine mRNA detected in the single-cell RNAseq study shown in Fig. 3. Proportion of cells in which vaccine mRNA was detected: values for individual mice and mean values ± SD.

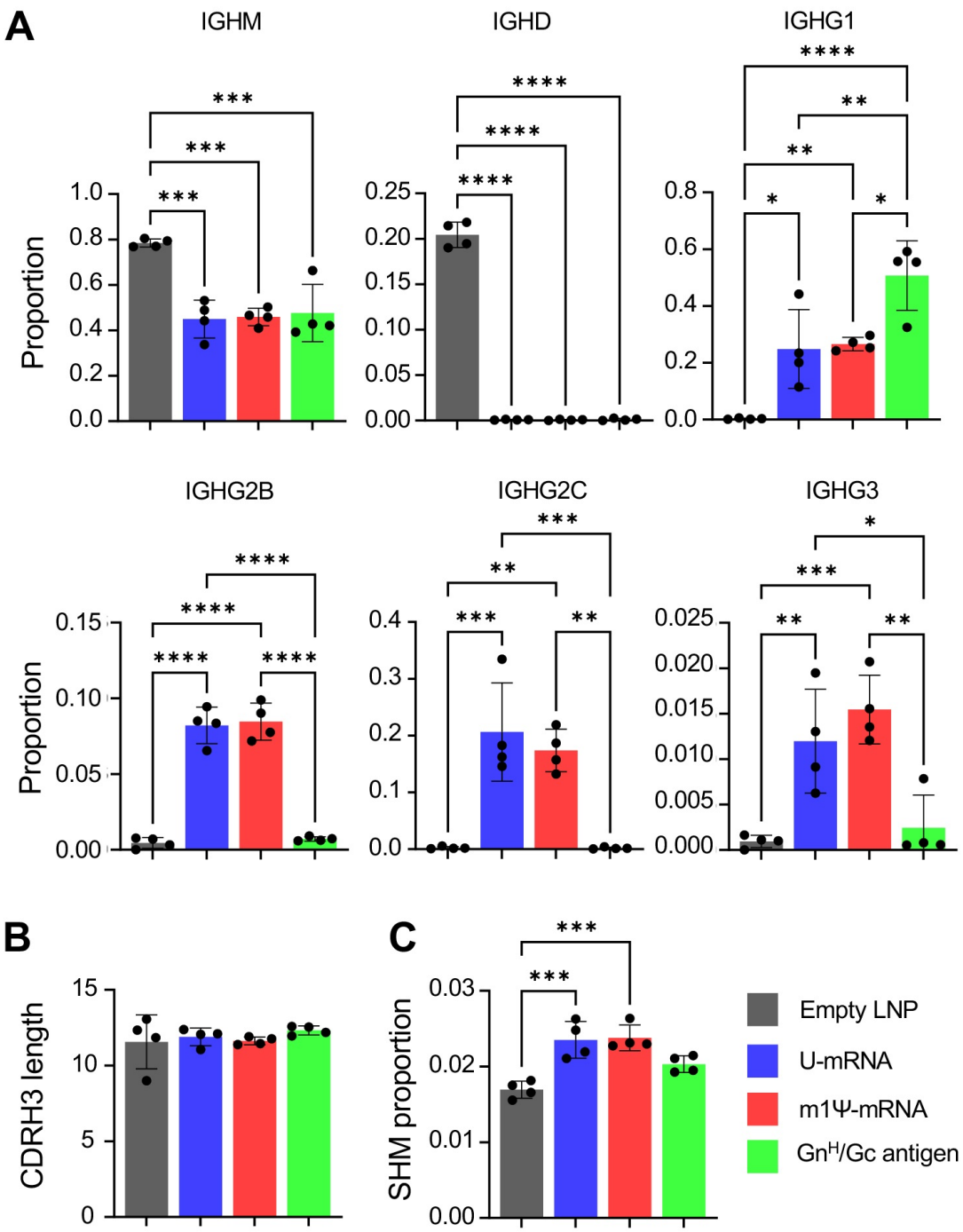

Figure 4

ANDV U-mRNA and m1Ψ-mRNA vaccines induce comparable class-switching and somatic hypermutation in mouse B cells. B cells from the mouse study presented in Fig. 3 were subjected to single-cell BCR RNA sequencing. A. Proportions of cells expressing the C region of heavy chain of various immunoglobulins. B. Average lengths of antibody heavy chains CDR3 regions (number of amino

acids). C. Average proportion of somatic hypermutation in CDRH3. Mean values ± SD, *p<0.05, **p<0.01, ***p<0.001, ****p<0.0001, unpaired two-sided Ttest.

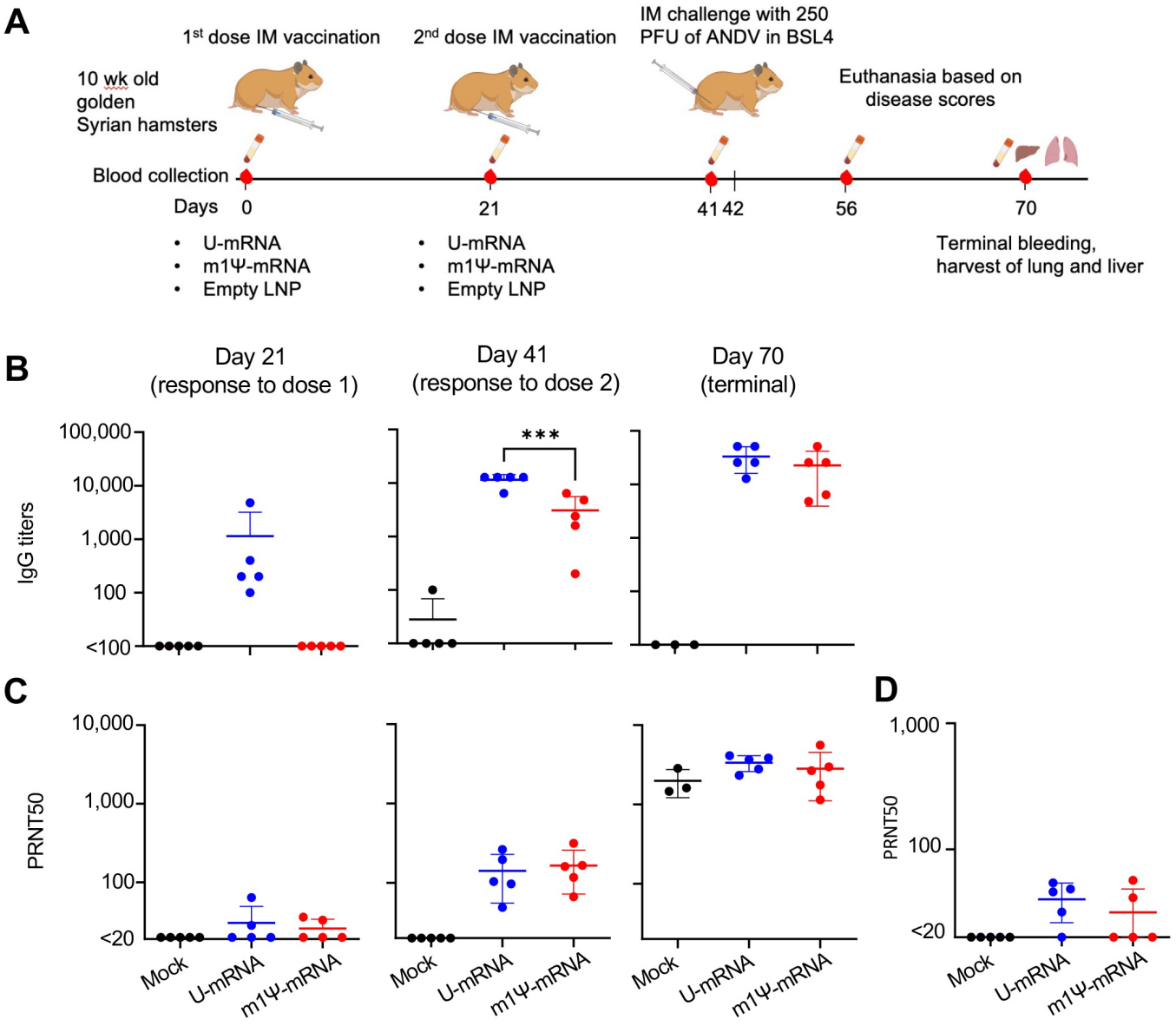

Figure 5

U-mRNA and Ψ-mRNA vaccines induce comparable binding and neutralizing antibody responses against ANDV. A. Schematic representation of the experiment: hamsters were immunized twice with ANDV mRNA vaccines and, along with naïve control, challenged with a lethal dose of ANDV. B. Binding IgG titers determined by ELISA with ANDV Gn/Gc antigen. C. ANDV neutralizing antibody titers in the hamster sera. D. Antibody neutralizing titers in hamster sera collected on day 41 determined against Sin Nombre virus. Optical densities at 450 nm (OD_{450}) of sera diluted 1:100. Mean values ± SD. SD bars are shown, ***p<0.001, unpaired twosided T-test.

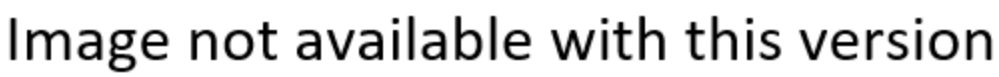

Figure 6

This image is not available with this version.

Supplementary Files

This is a list of supplementary files associated with this preprint. Click to download.

- SupplFiguresv10.pdf
- TableS1v1.docx